Proceedings of the ASME 2017 36th International Conference on Ocean, Offshore and Arctic Engineering
OMAE 2017
June 25-30, 2017, Trondheim, Norway

OMAE2017-61896

MODELING, PARAMETER IDENTIFICATION AND THRUSTER-ASSISTED POSITION MOORING OF C/S INOCEAN CAT I DRILLSHIP

Jon Bjørnø *
Norwegian University of Science and Technology (NTNU)
Sustainable Arctic Marine and Coastal Technology (SAMCoT)
Department of Marine Technology
NO-7491 Trondheim, Norway
Email: jon.bjorno@ntnu.no

Hans-Martin Heyn
Roger Skjetne
Norwegian University of Science and Technology (NTNU)
Sustainable Arctic Marine and Coastal Technology (SAMCoT)
Centre for Autonomous Marine Operations and Systems (AMOS)
Department of Marine Technology
NO-7491 Trondheim, Norway
Email: martin.heyn@ntnu.no, roger.skjetne@ntnu.no

Andreas R. Dahl
Preben Frederich
Norwegian University of Science and Technology (NTNU)
Centre for Autonomous Marine Operations and Systems (AMOS)
Department of Marine Technology
NO-7491 Trondheim, Norway
Email: andreas.r.dahl@ntnu.no, prebenf@stud.ntnu.no

ABSTRACT

A thruster-assisted position mooring (TAPM) system includes different control functions for stationkeeping and motion damping for a moored offshore vessel with assist from thrusters. It consists of a conventional mooring system and a dynamic positioning (DP) system. The thrusters are used to provide damping and some restoring to the vessel motion and compensate if line breakage occurs. The mooring system absorbs the main loads to keep the vessel in place. This paper presents a complete modeling, parameter identification, and control design for a 1:90 scaled TAPM model vessel. The numerical values for the different model parameters are identified from towing tests.

State-of-the-art TAPM control algorithms have been tested on the vessel in the Marine Control Laboratory (MC Lab), to see the behavior resulting from the different control algorithms. The presented experiments focus on the setpoint chasing algorithm, where the position setpoint slowly moves to the equilibrium position where the environmental loads are balanced by the mooring loads. This avoids conflicts between the mooring system and the control actions. If the environmental loads are too large so that the setpoint exceeds a user-defined safety radius, the setpoint is set to this radius and thruster forces grow to support the mooring system in counteracting the environmental loads to avoid line breakage. The experiments show that the vessel and setpoint chasing control algorithm behaves as expected, minimizing thruster usage and maximizing utilization of mooring system.

Keywords: C/S Inocean Cat I Drillship; Modeling; Parameter identification; Experimental results; Thruster-assisted position mooring; Thrust allocation; Setpoint chasing.

INTRODUCTION

Stationkeeping, i.e. maintaining a vessel's position fixed, is challenging in the ice and harsh weather of the Arctic. The capability is nevertheless essential for oil and gas exploration, as melting sea-ice is making the Arctic more accessible, the topic sees increased relevance. Dynamic positioning (DP) and thruster-assisted position mooring (TAPM) of turret-anchored

*Address all correspondence to this author.

vessels are possible concepts for Arctic deepwater offshore operations. The challenging ice and weather conditions in the Arctic make the control task more complicated, compared to a normal DP operation. The control system experiences new challenges due to the harsher conditions.

There exist multiple types of mooring systems, and the dynamic response of a moored vessel have been studied extensively. The mooring system contributes with the mean, restoring and damping forces to the moored vessel. The restoring and damping can be calculated by static and dynamic analysis of a catenary cable for the mooring lines [1–3]. The restoring force compensates the mean environmental loads are normally large in shallow waters, while the damping is increasing with water depth.

Several studies are published on control strategies for TAPM systems. These usually consist of manual, heading, and damping control, in addition to setpoint chasing [4–7]. Other control strategies like feedforward control and line breakage compensation also exist, e.g. [8].

Since most of the control strategies implicitly ensure that the mooring line tension is inside a safe margin, some authors have suggested control strategies that specifically take the line tension into account. Berntsen [9] proposed a control strategy that uses structural reliability measures for the mooring lines to restrict the vessel movement. Aamo and Fossen [6] presented another control strategy for line tension by changing the lengths of the mooring lines.

The objectives of this paper are modeling, parameter identification, and TAPM of C/S Inocean CAT I Drillship (CSAD), to provide the Norwegian University of Science and Technology (NTNU) with a new model vessel in the Marine Control Laboratory (MC Lab). More about CSAD can be found in [10, 11].

Principle of TAPM

A TAPM system consists of two parts, a conventional mooring system and a DP system. The mooring lines have a fixed position at the turret and seabed, which allows for the vessel to rotate freely about the turret. The DP of the system allows the vessel to use its thrusters to assist the mooring system. This allows the system to withstand harsher weather and faults that can occur during operations. The DP part also gives the ability to reduce the loads on the mooring lines by reducing the vessel motions and offset from the desired position, which also reduces the probability of loss of mooring lines.

The described configuration gives the vessel ability to weather-vane, which means that it can keep the position aligned with the environmental forces, where the turret is rotatable for transfer of loads between the vessel and the mooring lines.

TAPM is often also referred to as thruster-assisted mooring (TAM), position mooring (POSMOOR) or thruster-assisted mooring system (TAMS). In [12, pt.7], thrusters-assisted mooring is defined as:

> *"A stationkeeping system consists of mooring lines and thrusters. The thrusters contribute to control the structure's heading and to reduce mooring line forces and reduce structure offset."*

Historical Development of TAPM

The first vessel that introduced the TAPM system was Petrojarl in 1986 with its weather-vaning system [5]. From this year on, vessels were typically constructed with the turret inside 1/3 from the bow, and the placement of the accommodation could either be in behind the turret in the aft or fore in the front. Both solutions have their advantages and disadvantages, and the most marked disadvantage was when the accommodation block was placed in the front. This led to a large wind area that could deteriorate the weather-vaning ability of the vessel, which then required an active heading controller.

Aalbers et al. [5] states that the mooring line tension is strongly dependent on the water depth, turret location, and mooring line configuration. Due to the combination of the two mooring principles, thrusters to reduce loads on the mooring lines and a fluid swivel to allow continuous fluid flow during weather-vaning, more advanced control techniques were needed. This led to the development of more advanced TAPM controllers.

From 2007 until now, there has been increasing focus on the exploitation of oil and gas in deeper waters, and further north than before. This has made fixed platforms on the seabed impractical, at least for deep water operations. Instead, semi-submersibles and vessels with positioning systems have been widely used. The TAPM system is an economical solution for stationkeeping in deep water and in ice, due to that the vessel can withstand harsher conditions. Which again results in a longer operational windows.

Wassink and List [13] performed an analysis on development of solutions for Arctic offshore drilling. The results of this analysis show that the drillship with a TAPM solution is the best alternative when drilling in the Arctic. All alternatives have their advantages, but in two out of the three test categories considered by Wassink and List the drillship with TAPM showed the best results.

C/S INOCEAN CAT I DRILLSHIP

The hull of the original vessel, Statoil's Cat I Arctic Drillship, is designed by Inocean, and now these drawings have been used by Sintef Ocean to build a model of the same hull. The model hull is constructed in carbon fiber with brackets for the thrusters and with a deck (3-4 mm) out of acrylic fiber covering all of the bottom deck. Instead of a lowered mid-ship sec-

TABLE 1. C/S INOCEAN CAT I DRILLSHIP DIMENSIONS.

Description	Model data [m]	Full size data [m]
Length over all (L_{oa})	2.578	232
Breadth (B)	0.440	40
Depth molded (D)	0.211	19
Draft design (T)	0.133	12

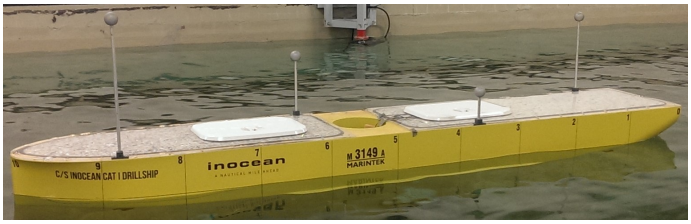

FIGURE 1. CSAD IN THE MC LAB.

tion, the deck is made planar. Due to limitations in the MC Lab, a scaling of 1:90 was chosen. Table 1 shows the scaled data of the vessel, and the vessel can be seen in Fig. 1.

The thruster system is placed corresponding to the Statoil's Cat I Arctic Drillship, and this consist of multiple parts; Aero-neut Precision Shcottel drive azimuth thruster, brushless OMA-2820-950 DC motor and Dynamixel MX-106R servo. There are six thrusters in total, and the respective places can be seen in Fig. 5.

CSAD has an inboard real-time embedded controller, the CompactRIO-9024 (cRIO) with different modules from National Instruments, to control the system. The cRIO is a combination of a real-time controller, reconfigurable I/O (RIO) modules, field-programmable gate array (FPGA) module, and an Ethernet expansion chassis. It is connected to the local LAN through a ASUS EA-N66 Wi-Fi bridge. To operate the vessel manually, a Sixaxis gamepad, in combination with Raspberry Pi 2 (RPi2), is used.

The system is powered from six 12 V 12 Ah lead batteries. Most of the equipment needs 12 V power, but there are some parts that need 5 V, such as the RPi2. These components are connected to either the USB outlet on the cRIO chassis or the 5 V outlet on cRIO modules.

To emulate a global navigation satellite system (GNSS) the MC Lab is equipped with a camera based real-time positioning system from Qualisys. CSAD is fitted with four silver spheres to obtain accurate 6 degree of freedom (DOF) position data by triangulation, within 1 mm precision, from this positioning system.

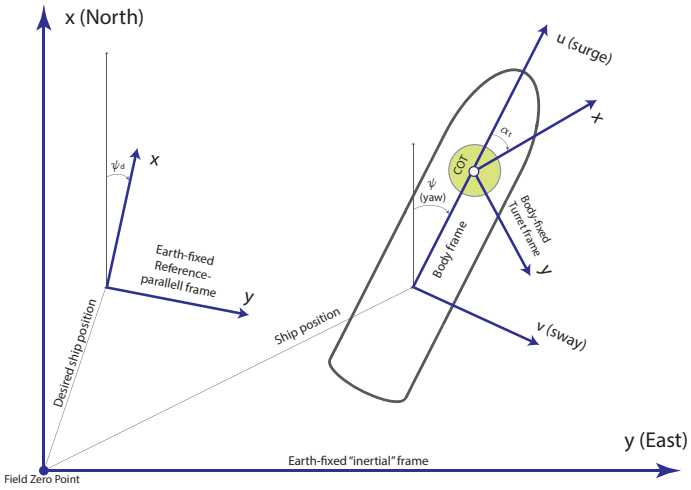

FIGURE 2. THE DIFFERENT REFERENCE FRAMES.

MATHEMATICAL MODELING

By using the proposed notations and reference frames in [4], the kinematics and kinetics for a TAPM vessel can be described as shown in the following subsections.

Kinematics

There are four different reference frames used in TAPM, as illustrated in Fig. 2.

- The earth-fixed frame {E} is located at mean sea-level with x-axis pointing north (N), y-axis east (E), and z-axis downwards (D). The origin is defined as Field Zero Point (FZP) located in the center of the turret when no environmental loads act on the vessel. The earth-fixed frame is in this paper represented by the basin-fixed frame.
- The reference-parallel frame {D} is the basin-fixed reference frame rotated to the desired heading angle ψ_d and origin in the desired (x_d, y_d) position. The desired position vector is the represented with $\boldsymbol{\eta}_d = [x_d, y_d, \psi_d]^\top$.
- The body-fixed frame {B} is fixed to the vessel body with the origin located in vessel origin (VO) of the hull. With x-axis positive forward, y-axis positive towards starboard and z-axis positive downwards.
- The turret-fixed frame {T} is fixed to the turret with the origin located in the center of the turret (COT) and rotated an angle α_t relative to the body x-axis.

The body-fixed linear and angular velocities of the vessel are related to the earth-fixed frame by the transformation

$$\dot{\boldsymbol{\eta}} = \mathbf{J}(\boldsymbol{\eta})\boldsymbol{\nu}, \tag{1}$$

where earth-fixed positions and body-fixed velocities are defined by $\boldsymbol{\eta} = [x, y, z, \phi, \theta, \psi]^\top$ and $\boldsymbol{\nu} = [u, v, w, p, q, r]^\top$, respec-

tively. The transformation matrix $\mathbf{J}(\boldsymbol{\eta})$ is given by

$$\mathbf{J}(\boldsymbol{\eta}) = \begin{bmatrix} \mathbf{J}_1(\boldsymbol{\eta}) & 0 \\ 0 & \mathbf{J}_2(\boldsymbol{\eta}) \end{bmatrix}, \tag{2}$$

$$\mathbf{J}_1(\boldsymbol{\eta}) = \begin{bmatrix} \mathrm{c}\psi\mathrm{c}\theta & -\mathrm{s}\phi+\mathrm{c}\theta+\mathrm{c}\phi\mathrm{s}\theta\mathrm{s}\phi & \mathrm{s}\psi\mathrm{s}\phi+\mathrm{c}\psi\mathrm{c}\phi\mathrm{s}\theta \\ \mathrm{s}\psi\mathrm{c}\theta & \mathrm{c}\psi\mathrm{c}\phi+\mathrm{s}\phi\mathrm{s}\theta\mathrm{s}\psi & -\mathrm{c}\psi\mathrm{s}\phi+\mathrm{s}\theta\mathrm{s}\psi\mathrm{c}\phi \\ -\mathrm{s}\theta & \mathrm{c}\theta\mathrm{s}\phi & \mathrm{c}\theta\mathrm{c}\phi \end{bmatrix}, \tag{3}$$

$$\mathbf{J}_2(\boldsymbol{\eta}) = \begin{bmatrix} 1 & \mathrm{s}\phi\mathrm{t}\theta & \mathrm{c}\phi\mathrm{t}\theta \\ 0 & \mathrm{c}\phi & -\mathrm{s}\phi \\ 0 & \mathrm{s}\phi/\mathrm{c}\theta & \mathrm{c}\phi/\mathrm{c}\theta \end{bmatrix}, \tag{4}$$

where $\mathrm{s}\cdot = \sin(\cdot), \mathrm{c}\cdot = \cos(\cdot), \mathrm{t}\cdot = \tan(\cdot)$.

Kinetics

The motion of a marine vessel is divided into two components; the low-frequency (LF) model and the wave-frequency (WF) model. These two models are combined through superposition. The details of the full 6 DOF model can be found in [14] and [15].

The LF model for a moored vessel is given by

$$\begin{aligned} \mathbf{M}_{\mathrm{RB}}\dot{\boldsymbol{\nu}} + \mathbf{M}_{\mathrm{A}}\dot{\boldsymbol{\nu}} + \mathbf{C}_{\mathrm{RB}}(\boldsymbol{\nu})\boldsymbol{\nu} + \mathbf{C}_{\mathrm{A}}(\boldsymbol{\nu}_r)\boldsymbol{\nu}_r + \mathbf{D}(\boldsymbol{\nu}_r)\boldsymbol{\nu}_r \\ = \boldsymbol{\tau}_{\mathrm{env}} + \boldsymbol{\tau}_{\mathrm{moor}} + \boldsymbol{\tau}_{\mathrm{thr}}, \end{aligned} \tag{5}$$

where $\mathbf{M}_{\mathrm{RB}}$ is the mass matrix, $\mathbf{M}_{\mathrm{A}}$ is the added mass matrix, $\mathbf{C}_{\mathrm{RB}}$ and $\mathbf{C}_{\mathrm{A}}$ are Coriolis and centripetal force matrices, $\boldsymbol{\nu}_r$ is the relative speed between the vessel and the water, which means that current is taken into account, $\mathbf{D}$ is the damping force function and $\boldsymbol{\tau}_{\mathrm{env}} = \boldsymbol{\tau}_{\mathrm{wind}} + \boldsymbol{\tau}_{\mathrm{wave2}}$ are the wind loads and 2nd order wave drift loads, respectively. The loads from the thrusters, $\boldsymbol{\tau}_{\mathrm{thr}}$, are controlled by the different control laws presented later.

Since this is a low-speed control application, we can neglect the Coriolis and centripetal terms because they are very small. Also, the non-linear parts of the damping term can be disregarded, because they are connected to higher order velocity-terms. Since we are using a simplified model, there might be some uncertainties and other changes not accounted for. By adding a bias model and removing $\boldsymbol{\tau}_{\mathrm{wind}}$, the uncertainties are accounted for. The influence of the wind is removed, because it is not implemented in the model. The LF model can then be rewritten to

$$\dot{\boldsymbol{\eta}} = \mathbf{J}(\boldsymbol{\eta})\boldsymbol{\nu}, \tag{6}$$

$$\dot{\mathbf{b}} = -\mathbf{T}_b\mathbf{b} + w_b, \tag{7}$$

$$\mathbf{M}\dot{\boldsymbol{\nu}} = -\mathbf{D}_{\mathrm{lin}}\boldsymbol{\nu} + \mathbf{J}(\boldsymbol{\eta})^\top\mathbf{b} + \boldsymbol{\tau}_{\mathrm{moor}} + \boldsymbol{\tau}_{\mathrm{thr}}, \tag{8}$$

where the bias force is $\mathbf{J}(\boldsymbol{\eta})^\top\mathbf{b} \approx \mathbf{D}_{\mathrm{lin}}\boldsymbol{\nu}_c + \boldsymbol{\tau}_{\mathrm{wave2}}$ and w_b is white noise.

Mooring Line Forces

For the LF motion model, a horizontal-plane spread mooring model is formulated as

$$\boldsymbol{\tau}_{\mathrm{moor}} = -\mathbf{J}^\top(\boldsymbol{\eta})\mathbf{g}_{\mathrm{moor}}(\boldsymbol{\eta} - \boldsymbol{\eta}_0) - \mathbf{d}_{\mathrm{moor}}\boldsymbol{\nu}, \tag{9}$$

where $\boldsymbol{\eta} \in \mathbb{R}^6$ is the position and $\boldsymbol{\eta}_0 \in \mathbb{R}^6$ is the equilibrium position where both are in Earth-fixed frame, and $\boldsymbol{\nu} \in \mathbb{R}^6$ is the velocities in body-fixed frame.

The restoring component, $\mathbf{g}_{\mathrm{moor}}$, can be formulated as

$$\mathbf{g}_{\mathrm{moor}} = \mathbf{T}(\boldsymbol{\beta})\mathbf{L}_p\boldsymbol{\tau}_H, \tag{10}$$

where $\boldsymbol{\tau}_H$ is the horizontal component of the tension and $\mathbf{L}_p$ is a diagonal coefficient matrix denoting the line breakage information. The mooring line configuration matrix is given by

$$\mathbf{T}(\boldsymbol{\beta}) = \begin{bmatrix} \cos\beta_1 & \cdots & \cos\beta_n \\ \sin\beta_1 & \cdots & \sin\beta_n \\ \bar{x}_1\sin\beta_1 - \bar{y}_1\cos\beta_1 & \cdots & \bar{x}_n\sin\beta_n - \bar{y}_n\cos\beta_n \end{bmatrix}, \tag{11}$$

where $\boldsymbol{\beta}$ is the mooring line orientation vector with angles between the mooring lines and the x-axis. $\bar{\mathbf{x}} = [\bar{x}_1, \cdots, \bar{x}_n]^\top$ and $\bar{\mathbf{y}} = [\bar{y}_1, \cdots, \bar{y}_n]^\top$ are the horizontal displacement of the mooring lines between the turret and the anchor cable. The mooring line characteristics can be found by software programs for marine slender structures, e.g. Mimosa [16], Riflex [17], and others.

Resulting Model

By combining the LF model in Eqn. 8 with the mooring line forces, we get the following:

$$\dot{\boldsymbol{\eta}} = \mathbf{J}(\boldsymbol{\eta})\boldsymbol{\nu}, \tag{12}$$

$$\dot{\mathbf{b}} = -\mathbf{T}_b\mathbf{b}(t) + w_b, \tag{13}$$

$$\mathbf{M}\dot{\boldsymbol{\nu}} = -\mathbf{D}\boldsymbol{\nu} - \mathbf{J}(\boldsymbol{\eta})^\top\mathbf{g}_{\mathrm{moor}}\boldsymbol{\eta} + \mathbf{J}(\boldsymbol{\eta})^\top\mathbf{b}(t) + \boldsymbol{\tau}_{\mathrm{thr}}, \tag{14}$$

where $\mathbf{D} = \mathbf{D}_{\mathrm{lin}} + \mathbf{d}_{\mathrm{moor}}$, $\mathbf{J}(\boldsymbol{\eta})^\top + \mathbf{b}(t) \approx \mathbf{D}_{\mathrm{lin}}\boldsymbol{\nu}_c + \boldsymbol{\tau}_{\mathrm{wave2}}$ and $\mathbf{g}_{\mathrm{moor}} = \mathbf{T}(\boldsymbol{\beta})\mathbf{L}_p\boldsymbol{\tau}_H$.

SYSTEM IDENTIFICATION 6 DOF MODEL

To get the system parameters for the 6 DOF vessel model, the MSS Toolbox [18] is used. Before this toolbox could be

used, it was necessary to do calculations with ShipX Vessel Responses Plug-In (VERES) [19]. The AutoCAD drawings of the Statoil's Cat I Arctic Drillship was converted to a ShipX file, and then scaled down by Froude scaling. In VERES the necessary vessel response calculations were done by setting the minimum wave period to a period that the vessel operates in, in this case 0.671 seconds, and filling in at least 10 periods in the same area. Then by using the result files from VERES with the functions in MSS Toolbox, `veres2vessel` and `vessel2ss`, the data files for the model were complete. This is then used in a Simulink model [20], by using the built-in block, `6 DOF DP model (zero speed model with fluid memory)`, from MSS Toolbox.

The entire procedure on how to go from a ShipX model to get the system parameters in MATLAB [21] is described by [22].

For the mooring system, a Simulink model made by [23] is used. This model is in full scale, so it was necessary to scale it down to fit the CSAD model. This scaling was done by using Froude scaling laws.

SYSTEM IDENTIFICATION 3 DOF MODEL

Since this vessel will be used for other applications than just TAPM, e.g. DP, maneuvering, etc., a 3 DOF model is needed. This requires some modifications to Eqn. 8. The resulting model becomes

$$\dot{\boldsymbol{\eta}} = \mathbf{R}(\psi)\boldsymbol{\nu}, \tag{15}$$

$$\mathbf{M}\dot{\boldsymbol{\nu}} = -\mathbf{C}(\boldsymbol{\nu})\boldsymbol{\nu} - \mathbf{D}(\boldsymbol{\nu})\boldsymbol{\nu} + \boldsymbol{\tau}_{\text{env}} + \boldsymbol{\tau}_{\text{thr}}, \tag{16}$$

where $\boldsymbol{\eta} = [x, y, \psi]^\top \in \mathbb{R}^3$, $\boldsymbol{\nu} = [u, v, r]^\top \in \mathbb{R}^3$ and $\boldsymbol{\tau} = [X, Y, N]^\top \in \mathbb{R}^3$. The rotation matrix $\mathbf{R}(\psi)$ is given by

$$\boldsymbol{R(\eta)} = \mathbf{R}(\psi) = \begin{bmatrix} \cos\psi & -\sin\psi & 0 \\ \sin\psi & \cos\psi & 0 \\ 0 & 0 & 1 \end{bmatrix}. \tag{17}$$

The mass and Coriolis matrices are given as

$$\mathbf{M} = \begin{bmatrix} m - X_{\dot{u}} & 0 & 0 \\ 0 & m - Y_{\dot{v}} & mx_g - Y_{\dot{r}} \\ 0 & mx_g - Y_{\dot{r}} & I_z - N_{\dot{r}} \end{bmatrix} = \mathbf{M}^\top > 0, \tag{18}$$

$$\mathbf{C}(\boldsymbol{\nu}) = \begin{bmatrix} 0 & -mr & Y_{\dot{v}}v + (Y_{\dot{r}} - mx_g)r \\ mr & 0 & -X_{\dot{u}}u \\ -Y_{\dot{v}}v - (Y_{\dot{r}} - mx_g)r & X_{\dot{u}}u & 0 \end{bmatrix}, \tag{19}$$

TABLE 2. CSAD RIGID BODY AND ADDED MASS PARAMETERS.

Rigid Body		Added mass	
Parameter	Value	Parameter	Value
m	128	$X_{\dot{u}}$	3.26
I_z	62	$Y_{\dot{v}}$	28.9
x_g	0	$Y_{\dot{r}}$	0.525
		$N_{\dot{v}}$	0.157
		$N_{\dot{r}}$	14

where the parameter values are given in Tab. 2. The damping matrix is given as

$$\mathbf{D}(\boldsymbol{\nu}) = -\begin{bmatrix} d_{11}(u) & 0 & 0 \\ 0 & d_{22}(v,r) & d_{23}(v,r) \\ 0 & d_{32}(v,r) & d_{33}(v,r) \end{bmatrix}, \tag{20}$$

where the damping components are:

$$d_{11}(u) = X_u + X_{|u|u}|u| + X_{uuu}u^2, \tag{21}$$

$$d_{22}(v,r) = Y_v + Y_{|v|v}|v| + Y_{vvv}v^2 + Y_{|r|v}|r|, \tag{22}$$

$$d_{23}(v,r) = Y_r + Y_{|v|r}|v| + Y_{|r|r}|r| + Y_{rrr}r^2, \tag{23}$$

$$d_{32}(v,r) = N_v + N_{|v|v}|v| + N_{vvv}v^2 + N_{|r|v}|r|, \tag{24}$$

$$d_{33}(v,r) = N_r + N_{|v|r}|v| + N_{|r|r}|r| + N_{rrr}r^2, \tag{25}$$

with parameters to be decided in the next section.

Drag Coefficients

In order to estimate the vessel damping term in Eqn. 20, for the 3 DOF model, towing tests in surge, sway and yaw were performed in the MC Lab. The test setup is shown in Fig. 3, where force rings are fitted in the stern and on the side to measure the force in different directions. The springs are there to keep the vessel straight and eliminate oscillations when forces are acting on the vessel in surge and sway. The test set-up for finding the yaw moment has a minor change from the surge and sway set-up, the aft spring and force ring have switched places. The tests were performed by towing and rotating the vessel with different velocities. To obtain the resistance forces on the hull, all thrusters were directed along the x-axis backwards to reduce the resistance.

The data series collected from the towing tests have been post-processed in MATLAB. By using a curve fitting tool, the

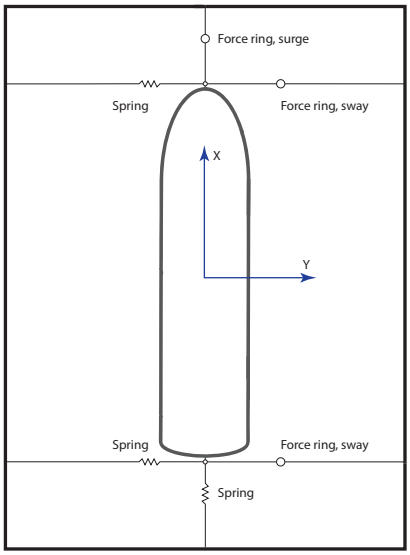

FIGURE 3. **THE TOWING SETUP FOR CSAD.**

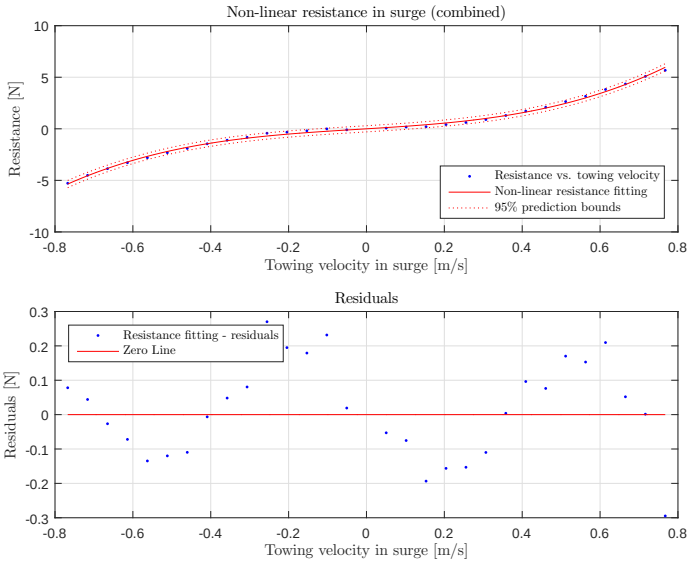

FIGURE 4. **DRAG FORCES ACTING ON THE HULL IN SURGE.**

damping terms as a function of velocity in surge, sway and yaw have been found. The surge results can be seen in Fig. 4, the sway and yaw results can be found in [10].

From these results the linear and nonlinear drag coefficients for CSAD, in surge, sway and yaw, can be found. The results are based on a cubic function, with the form $y = ax^3 + bx^2 + cx$, and zero resistance at zero velocity. Table 3 lists the resulting coefficients. The coupling terms in sway and yaw were not obtained from these tests. To have an estimate of these values, the coupling terms from a similar model vessel were used.

TABLE 3. **DRAG COEFFICIENTS IN SURGE, SWAY AND YAW WITH COUPLING TERMS.**

Surge		Sway		Yaw	
Parameter	Value	Parameter	Value	Parameter	Value
X_u	-2.33	Y_v	-4.67	N_v	0
X_{uu}	0	Y_{vv}	0.398	N_{vv}	-0.209
X_{uuu}	-8.56	Y_{vvv}	-313	N_{vvv}	0
X_v	0	Y_r	-7.25	N_r	-0.0168
X_{vv}	0	Y_{rr}	-3.45	N_{rr}	-0.0115
X_{vvv}	0	Y_{rrr}	0	N_{rrr}	-0.000358
		Y_{rv}	-0.805	N_{rv}	0.08
		Y_{vr}	-0.845	N_{vr}	0.08

Note: With this specific damping matrix, the model is only valid for low speed.

THRUST PARAMETER IDENTIFICATION

Many of the parameters such as dimensions, maximum thrust and turn rate given by Inocean and Rolls-Royce are scaled directly down with Froudes scaling laws, as seen in Tab. 4 and Fig. 5, and used as constraints for the thrusters. The effect of that CSAD's propeller dimension is a bit smaller than the scaled dimension, found by Froudes scaling, is minimal.

Not all parameters and constraints are possible to find directly. The remaining parameters are therefore approximated using known theories or directly measured from the model through testing. In the following section, one of the main tests conducted is elaborated.

Bollard Pull

The bollard pull method is normally used to find maximum thrust possible to produce. By using the same principle with incremental steps instead, the pulse-width modulation (PWM) signal used to control thrust can be mapped correctly with regards to thruster control. Furthermore, by combining Eqn. 26 and 27, found by [24], with the results for shaft speed and thrust, an approximate value for each thrust and torque coefficient can be found.

$$K_T = \frac{T_a}{\text{sign}(n)\rho D^4 n^2}, \tag{26}$$

$$K_Q = \frac{Q_a}{\text{sign}(n)\rho D^5 n^2}. \tag{27}$$

TABLE 4. SCALED PARAMETERS USED FOR CSAD.

Name	Real vessel	Model vessel	
Max shaft speed	2.38	94.9	[RPS]
Power	6 000 000	0.868	[W]
Propeller Diameter	4.2	0.030	[m]
Steering speed	12	114	[deg/s]
Max Torque	95 500	0.0015	[Nm]
Max Thrust	1 095 000	1.50	[N]

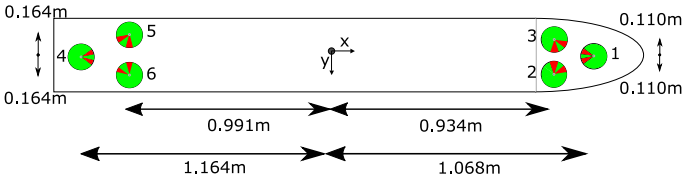

FIGURE 5. DIMENSION AND CONSTRAINTS ON CSAD.

THRUSTER CONTROL

Mapping of corresponding thrust controller to a PWM signal found by bollard pull test are also implemented in the thruster control. Through theory described by [15], the thruster control system is modeled with regards to shaft speed, torque and/or power control together with scaled constraints on thruster capacity. By adding a multiport switch with constraints on singularity handling, the different controllers can be switched online.

THRUSTER ALLOCATION

There are many different algorithms to solve the thrust allocation problem. For CSAD, a constrained pseudoinverse solver is used. According to [25], the method used on CSAD can be described as

$$\mathbf{u}_d = \mathbf{K}\mathbf{B}^{\dagger}(\alpha)\boldsymbol{\tau}_c - \mathbf{s}, \tag{28}$$

where $\mathbf{B}^{\dagger}(\alpha)$ is the pseudoinverse configuration with 3 DOF and 6 thrusters, $\boldsymbol{\tau}_c$ are the commanded generalized forces, $\mathbf{s}$ is the slack variable, which is generally given as a very small value to ensure no singularities and only small deviations in optimal thrust. For CSAD, the slack variable is set to $\mathbf{s} = 1 \times 10^{-5}$. $\mathbf{u}_d$ is desired thrust for each thruster. $\mathbf{K}$ is a user defined weighting function which ensures no thrust is produced when a thruster is inside a forbidden zone, indicated with red marking on each thruster in Fig. 5. $\mathbf{B}^{\dagger}(\alpha)$ is the Moore-Penrose pseudoinverse

$$\mathbf{B}^{\dagger}(\alpha) = \mathbf{B}\mathbf{S}^{\dagger}\mathbf{U}^{\top}, \tag{29}$$

where $\mathbf{S}^{\dagger}$ is a diagonal 3×3 matrix containing the singular values of the thruster configuration matrix, $\mathbf{B}(\alpha)$. For CSAD, the thruster configuration matrix can be written as

$$\boldsymbol{B}_{3\times 6}(\boldsymbol{\alpha}) = \begin{bmatrix} \cos(\alpha_1) & \sin(\alpha_1) & l_{x1}\sin(\alpha_1) - l_{y1}\cos(\alpha_1) \\ \cos(\alpha_2) & \sin(\alpha_2) & l_{x2}\sin(\alpha_2) - l_{y2}\cos(\alpha_2) \\ \cos(\alpha_3) & \sin(\alpha_3) & l_{x3}\sin(\alpha_3) - l_{y3}\cos(\alpha_3) \\ \cos(\alpha_4) & \sin(\alpha_4) & l_{x4}\sin(\alpha_4) - l_{y4}\cos(\alpha_4) \\ \cos(\alpha_5) & \sin(\alpha_5) & l_{x5}\sin(\alpha_5) - l_{y5}\cos(\alpha_5) \\ \cos(\alpha_6) & \sin(\alpha_6) & l_{x6}\sin(\alpha_6) - l_{y6}\cos(\alpha_6) \end{bmatrix}^{\top}, \tag{30}$$

where α_i represents the angle for each thruster, l_x and l_y represents the x and y coordinates as seen on Fig. 5.

By ensuring large singular values are set to zero, the thruster will not produce excessive thrust if they are at a poor angle. By controlling $\mathbf{S}^{\dagger}$, weighting can be given depending on how the thrusters angles are positioned at a given time. For CSAD, values of $\mathbf{S}^{\dagger}$ are chosen to be zero whenever one of its values are ten times as high as the others. From [11], the effect of different weighting values of $\mathbf{S}^{\dagger}$ through simulation can be seen.

Furthermore, in order to find the optimal angle for each thruster, an extended version of Eqn. 28 is used where $\mathbf{u}_d$ describes the optimal desired thrust in both x- and y-direction for each thruster. By using the trigonometric relation, the optimal angle for each thruster can be found by

$$\alpha_i = \text{atan2}(u_{iy}, u_{ix}), \tag{31}$$

where u_{iy} is the y-component and u_{ix} is the x-component.

Having α_i, then check against forbidden zones and limited by maximum rotation rate, the new thruster angle is found.

CONTROLLER DESIGN

The control objective is to bring the vessel to the desired position and keep it there. This can be expressed mathematically as

$$\lim_{t\to\infty} \boldsymbol{\eta}(t) = \boldsymbol{\eta}_d. \tag{32}$$

Heading Control

The heading controller adjusts the vessel heading towards the environmental forces to reduce the loads on the vessel and

its mooring system. The heading controller can be described mathematically as a PID controller [26]

$$\boldsymbol{\tau}_{\text{PID}}^{\psi} = -\mathbf{H}_{\psi}\mathbf{K}_{\text{I}}\mathbf{R}(\psi)^{\top}\boldsymbol{\xi} - \mathbf{H}_{\psi}\mathbf{K}_{\text{P}}\mathbf{R}(\psi)^{\top}(\boldsymbol{\eta}-\boldsymbol{\eta}_d) - \mathbf{H}_{\psi}\mathbf{K}_{\text{D}}(\boldsymbol{\nu}-\boldsymbol{\nu}_d), \quad (33)$$

where $\mathbf{H}_{\psi} = \text{diag}(0,0,1)$, since only the heading is subjected to control, $\mathbf{K}_{\text{P}}$,$\mathbf{K}_{\text{I}}$ and $\mathbf{K}_{\text{D}}$ are the controller gain matrices and $\dot{\boldsymbol{\xi}} = \boldsymbol{\eta}-\boldsymbol{\eta}_d$.

Surge/Sway Damping and Restoring

The surge/sway controller dampens the unwanted large oscillatory motion in surge and sway, and reduces the stress on the mooring system. The surge/sway damping and restoring controller can be described mathematically as a PD-controller [26]

$$\boldsymbol{\tau}_{\text{PD}}^{xy} = -\mathbf{H}_{xy}\mathbf{K}_{\text{P}}\mathbf{R}(\psi)^{\top}(\boldsymbol{\eta}-\boldsymbol{\eta}_d) - \mathbf{H}_{xy}\mathbf{K}_{\text{D}}(\boldsymbol{\nu}-\boldsymbol{\nu}_d), \quad (34)$$

where $\mathbf{H}_{xy} = \text{diag}(1,1,0)$ and $\mathbf{K}_{\text{P}}$, $\mathbf{K}_{\text{D}}$ are the controller gain matrices.

Setpoint Chasing by Lowpass Filtering

The objective of this controller is to keep the thrust at its minimum by changing the setpoint continuously to the equilibrium position where the environmental loads are balanced by the mooring forces. The proposed setpoint chasing algorithm from [7] is presented as

$$\dot{\boldsymbol{\eta}}_d = -\boldsymbol{\Lambda}\boldsymbol{\eta}_d + \boldsymbol{\Lambda}\boldsymbol{\eta}_{xy}, \quad (35)$$

where $\dot{\boldsymbol{\eta}}_d \in \mathbb{R}^2$ is the system dynamics of the desired LF position of the vessel and $\boldsymbol{\Lambda} \in \mathbb{R}^{2\times 2}$ is the first-order diagonal and non-negative filter gain matrix with the cutoff frequencies $1/T_{s_i}$ given by

$$\boldsymbol{\Lambda} = \text{diag}(1/T_{s_1}, 1/T_{s_2}). \quad (36)$$

This then continuously produces a new setpoint for the controller, so that the controller commands minimal force, until the critical radius is reached. If the environmental loads move the vessel out of bounds, then $\boldsymbol{\eta}_d = \boldsymbol{\eta}_{cr}$. The controller is just a regular PID controller that can be represented as

$$\boldsymbol{\tau}_{\text{PID}} = -\mathbf{K}_{\text{P}}\mathbf{R}(\psi)^{\top}(\boldsymbol{\eta}-\boldsymbol{\eta}_d) - \mathbf{K}_{\text{I}}\mathbf{R}(\psi)^{\top}\boldsymbol{\xi} - \mathbf{K}_{\text{D}}(\boldsymbol{\nu}-\boldsymbol{\nu}_d), \quad (37)$$

where $\dot{\boldsymbol{\xi}} = \boldsymbol{\eta}-\boldsymbol{\eta}_d$ and $\mathbf{K}_{\text{P}}$, $\mathbf{K}_{\text{I}}$ and $\mathbf{K}_{\text{D}}$ are the controller gain matrices. To get a clearer view of how the the setpoint generator works, a block diagram is shown in Fig. 6.

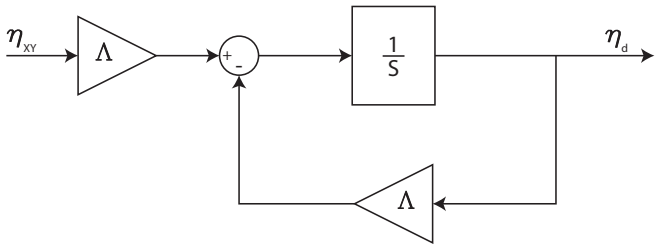

FIGURE 6. **SETPOINT GENERATOR BLOCK DIAGRAM.**

OBSERVER DESIGN

To avoid either noisy or incomplete measurements from the positioning system in the MC Lab, an observer is used to estimate these. By applying the assumptions given in [14] and [7] for the LF model, we get the following non-linear passive observer equations

$$\dot{\hat{\boldsymbol{\xi}}} = \mathbf{A}_{\text{w}}\hat{\boldsymbol{\xi}} + \mathbf{K}_1(\omega_0)\tilde{\mathbf{y}}, \quad (38)$$

$$\dot{\hat{\boldsymbol{\eta}}} = \mathbf{R}(\psi)\hat{\boldsymbol{\nu}} + \mathbf{K}_2\tilde{\mathbf{y}}, \quad (39)$$

$$\dot{\hat{\mathbf{b}}} = -\mathbf{T}_{\text{b}}\hat{\mathbf{b}} + \mathbf{K}_3\tilde{\mathbf{y}}, \quad (40)$$

$$\mathbf{M}\dot{\hat{\boldsymbol{\nu}}} = -\mathbf{D}\hat{\boldsymbol{\nu}} + \mathbf{R}(\psi)^{\top}\hat{\mathbf{b}} - \mathbf{R}(\psi)^{\top}\mathbf{G}_{\text{moor}}\hat{\boldsymbol{\eta}} + \boldsymbol{\tau}_{\text{thr}} + \mathbf{R}(\psi)^{\top}\mathbf{K}_4\tilde{\mathbf{y}}, \quad (41)$$

$$\mathbf{y} = \hat{\boldsymbol{\eta}} + \mathbf{C}_{\text{w}}\hat{\boldsymbol{\xi}}, \quad (42)$$

where $\tilde{\mathbf{y}} = \mathbf{y}-\hat{\mathbf{y}}$ is the estimation error, $\mathbf{K}_1(\omega_0) \in \mathbb{R}^{6\times 3}$, $\mathbf{K}_{2,3,4} \in \mathbb{R}^{3\times 3}$ are the observer gains, $\mathbf{C}_{\text{w}} \in \mathbb{R}^{3\times 6}$ is a constant matrix describing the sea state. $\mathbf{G}_{\text{moor}}$ and $\mathbf{D}_{\text{moor}}$ are linearized mooring stiffness and damping matrices assumed to only contribute in the horizontal-plane.

EXPERIMENTAL RESULTS

To show how the vessel behaves with a TAPM controller, the setpoint chasing controller is chosen. The vessel turret is fitted with four mooring lines evenly spread on the bottom. These mooring lines have springs attached on both connector points to give them restoring capabilities. The thrusters will dampen the vessel movement, since the damping capabilities for the mooring lines are small. Figures 7 and 8 show the behavior of the vessel with desired heading $\psi_d = 5°$, in irregular waves that corresponds to $H_s = 4$ meters in full scale. From Fig. 9, it can be seen that the controller uses minimum thrust inside the safety circle, and stationkeeping when the vessel reaches the circle limit. As seen from the yaw plot in Fig. 7 and 9, there is a problem stabilizing the heading, and it is oscillating around desired heading.

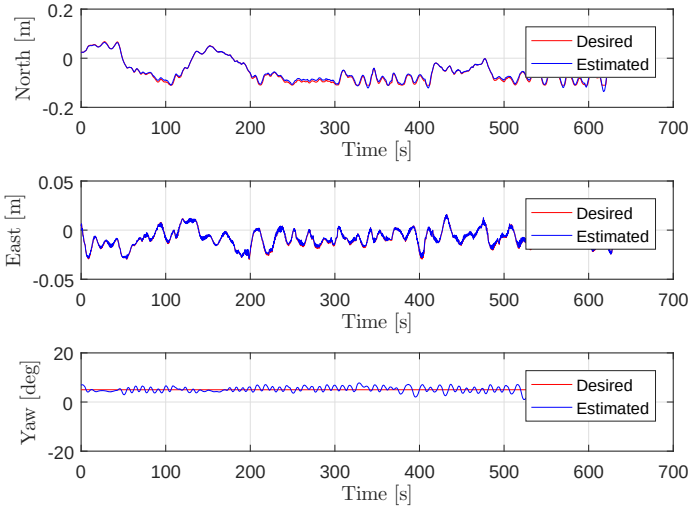

FIGURE 7. **POSITION OVER TIME IN SURGE, SWAY AND YAW.**

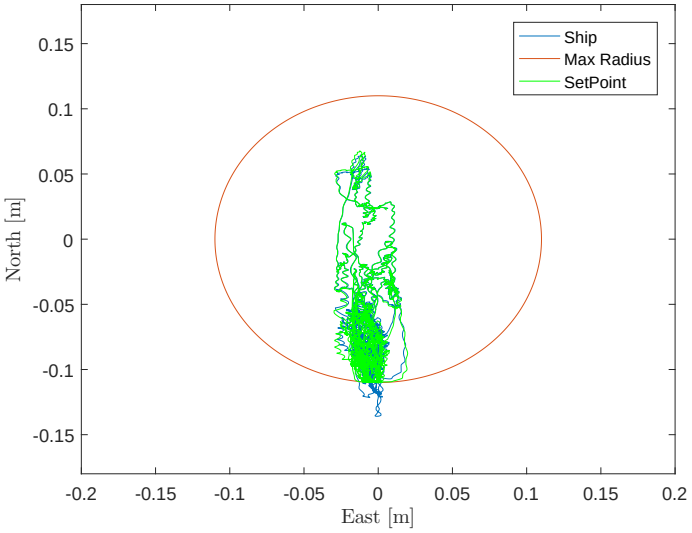

FIGURE 8. **XY-PLOT OF THE POSITION.**

DISCUSSION

Presented in Fig. 7 and 8, the setpoint generated path for the vessel works very well. The vessel is controlled accordingly to the setpoint, and the thrust is kept to its minimum inside the safety circle. There may be some improvements to the setpoint chasing algorithm, by tuning the non-negative filter gain matrix better, but improvements would be infinitesimal.

The reason for the oscillations in heading, as seen in the yaw plot of Fig. 7, is discussed later in experimental uncertainties.

Since the controller is reactive, which means that the incident has to happen before the controller react, there will be a deviation from the desired position. This is caused by the varying wave height that encounters the vessel. An approach that may remove the deviation, are proactive controllers. These controllers have inputs on how the environmental loads will act, and respond with the correct thrust to withstand these loads at impact. More on this topic, and more effective stationkeeping in ice, is presented in [27].

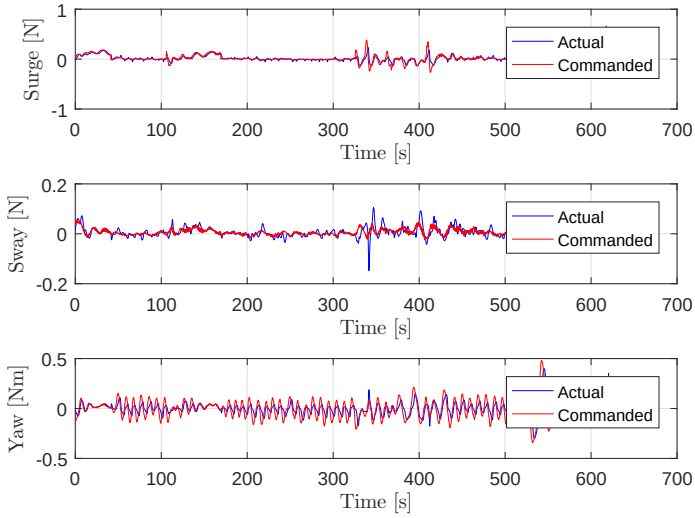

FIGURE 9. **THRUST OVER TIME IN SURGE, SWAY AND YAW.**

Experimental Uncertainties

There are several uncertainties in this kind of experiments with a scale model. First of all, the positioning system in the MC Lab is extremely sensitive regarding the silver spheres on the vessel, and the connection can easily be lost while running the experiments. This can create deviations in the position, or may require a new run due to loss of signal.

Another uncertainty can be the thrust allocation implemented in the model, in order to account for the mappings between thrust output and hardware on the model. This may be the reason for the heading deviation in the results.

As a general remark to the experiments, it may be hard to tune the different controllers and observers. During the experiments, this has been done manually by trial and error, until the best and most stable response was achieved.

CONCLUSION

The CSAD has been designed, constructed and assembled. This has now given NTNU a new research platform in MC Lab. However, work still remains to improve the CSAD, to open up the possibility for more complex control algorithms. The model is easy to operate and control, and the combination with cRIO, VeriStand and Simulink give a good platform to work with.

The performance of the vessel was not perfect, but could have been improved by using more time on tuning the different parameters and controller. Sorting out the error in the thrust allocation could also have improved the performance. All in all, a simulation model has been derived, based on the CSAD, and a functioning TAPM system was demonstrated.

ACKNOWLEDGMENT

This work was supported by the Research Council of Norway through the CRI SAMCoT, project no. 203471, and the CoE AMOS, project no. 223254. We also wish to thank Inocean AS for sharing their design drawings for construction of the ship hull, and Statoil ASA for supporting the development.

REFERENCES

[1] Triantafyllou, M., Yue, D., and Tein, D., 1994. "Damping Of Moored Floating Structures". In Offshore Technology Conference, Society of Petroleum Engineers (SPE).

[2] Ormberg, H., and Larsen, K., 1998. "Coupled analysis of floater motion and mooring dynamics for a turret-moored ship". *Appl. Ocean Res.,* ***20***(1-2), pp. 55–67.

[3] Triantafyllou, M. S., 1990. *Cable mechanics with marine applications*. Department of Ocean Engineering, Massachusetts Institute of Technology, Cambridge, MA 02139, USA. Lecture Notes.

[4] Strand, J. P., Sørensen, A. J., and Fossen, T. I., 1998. "Design of automatic thruster assisted mooring systems for ships". *Modeling, Identification and Control (MIC),* ***19***(2), pp. 61–75.

[5] Aalbers, A., Janse, S., and Boom, W. D., 1995. "DP Assisted and Passive Mooring for FPSO's". *Offshore Technology Conference*.

[6] Aamo, O. M., and Fossen, T. I., 1999. "Controlling line tension in thruster assisted mooring systems". *Proceedings of the 1999 IEEE International Conference on Control Applications*, pp. 1104–1109.

[7] Nguyen, D. T., and Sørensen, A. J., 2009. "Setpoint Chasing for Thruster-Assisted Position Mooring". *IEEE J. Oceanic. Eng.,* ***34***(4), p. 548–558.

[8] Ren, Z., Skjetne, R., and Hassani, V., 2015. "Supervisory control of line breakage for thruster-assisted position mooring system". *IFAC-PapersOnLine,* ***48***(16), pp. 235–240.

[9] Berntsen, P. I. B., 2008. "Structural Reliability Based Position Mooring". PhD thesis, Norwegian University of Science and Technology, Trondheim, Norway.

[10] Bjørnø, J., 2016. "Thruster-Assisted Position Mooring of C/S Inocean Cat I Drillship". Master's thesis, Norwegian University of Science and Technology, Trondheim, Norway.

[11] Frederich, P., 2016. "Constrained Optimal Thrust Allocation for C/S Inocean Cat I Drillship". Master's thesis, Norwegian University of Science and Technology, Trondheim, Norway.

[12] International Organization for Standardization (ISO), 2013. Petroleum and natural gas industries - specific requirements for offshore structures. Tech. Rep. ISO/TC 67/SC 7.

[13] Wassink, A., and List, R. V. D., 2013. "Development of Solutions for Arctic Offshore Drilling". *SPE Arctic and Extreme Environments Technical Conference and Exhibition*.

[14] Fossen, T. I., 2011. *Handbook of Marine Craft Hydrodynamics and Motion Control*. John Wiley & Sons, Ltd.

[15] Sørensen, A. J., 2013. *Marine Control Systems: Propulsion and Motion Control of Ships and Ocean Structures*, 3 ed. Norwegian University of Science and Technology, Trondheim, Norway. Report UK-13-76.

[16] DNV GL. Mimosa [Software]. https://www.dnvgl.com/services/mooring-system-and-individual-mooring-line-analysis-mimosa-2313.

[17] DNV GL. Riflex [Software]. https://www.dnvgl.com/services/riser-analysis-riflex-2312.

[18] Fossen, T. I., and Perez, T., 2004. Marine Systems Simulator (MSS). http://www.marinecontrol.org.

[19] Sintef, 2015. ShipX [Software]. Retrived from https://www.sintef.no/en/software/shipx/.

[20] The MathWorks, Inc., 2015. Simulink [Software]. Retrived from http://www.mathworks.com/products/simulink.html.

[21] The MathWorks, Inc., 2015. MATLAB [Software]. Retrived from https://se.mathworks.com/products/matlab.html.

[22] Fossen, T. I., 2008. Description of MSS Vessel Models: Configuration Guidelines for Hydrodynamic Codes. http://www.marinecontrol.org/pdf/2008_06_19_MSS_vessel_models.pdf.

[23] Ren, Z., 2015. "Fault-Tolerant Control of Thruster-Assisted Position Mooring System". Master's thesis, Norwegian University of Science and Technology, Trondheim, Norway.

[24] van Lammeren, W. P. A., van Manen, J. D., and Oosterveld, M. W. C., 1969. "The Wagening B-Screw Series". SNAME.

[25] Sørdalen, O. J., 1997. "Optimal Thrust Allocation for Marine Vessels". *Control Engineering Practice,* ***5***(9), pp. 1223–1231.

[26] Nguyen, D. T., and Sørensen, A. J., 2009. "Switching control for thruster-assisted position mooring". *Control Eng. Pract.,* ***17***(9), p. 985–994.

[27] Skjetne, R., Imsland, L., and Løset, S., 2014. "The Arctic DP Research Project: Effective Stationkeeping in Ice". *Modeling, Identification and Control (MIC),* ***35***(4), pp. 191–210.